Hot-Electron Spectroscopy of Bloch Electrons in High-Order Minibands in Semiconductor Superlattices

P. England, J. R. Hayes, E. Colas, and M. Helm
Bellcore, 331 Newman Springs Road, Red Bank, New Jersey 07701-7040
(Received 17 May 1989)

We inject electrons at arbitrary energy into the band structure of a GaAs/AlGaAs semiconductor superlattice. The electrons traverse a finite number of periods and are then analyzed for the electron momentum distribution using a hot-electron spectrometer. By this technique, we are able to give the first demonstration of miniband conduction through high-order minibands. We relate the transmission and energy-loss characteristic to tight-binding models of the superlattice.

PACS numbers: 71.25.Tn, 72.20.Ht, 73.40.Gk, 73.40.Lq

Semiconductor superlattices provide an ideal system in which to study band transport in periodic materials in a range of parameter space inaccessible in natural structures.[1] By adjusting the well and barrier thickness and composition, it is possible to tailor the electronic states from being localized to being extended "miniband" states,[2] and experimentalists have not only revealed the formation of bands,[3] they have also been able to explore a range of transport processes from hopping conduction to band transport.[2,4]

A key issue is coherent or miniband transport. Although there have been convincing demonstrations of miniband transport by techniques as diverse as cyclotron resonance,[5] time of flight,[6,7] and tunneling studies,[8,9] they all suffer from the same limitation that the electrons (or holes) have been confined to the bottom of the lowest-lying miniband. It is also important to address the possibility of hot-electron transport in high-lying minibands, where the bandwidths are larger and therefore less subject to localization by unavoidable fluctuations, but the mean free path can be curtailed by inelastic processes such as phonon or plasmon emission. In this case we can envisage situations where the electronic states are delocalized, but the mean free path of electrons is of the order of the superlattice period.

In this Letter, we report the first experimental observation of Bloch transport in high-lying minibands (the second, third, and fourth) in semiconductor superlattices. We have performed measurements on a variety of superlattices, sandwiched between a variable-energy electron injector on one side, and an electron spectrometer on the other (inset, Fig. 1).[10,11] With this new technique we may unambiguously identify electrons which traverse the superlattice in a single miniband. It also allows the first measurement of scattering rates and mean free paths of hot carriers in such an artificial periodic system. We have modeled the system assuming an infinite superlattice, and obtain excellent agreement with our data. This demonstrates the remarkable result that even in a finite system with strong scattering, the electrons are essentially described by the infinite-system dispersion relation.

In detail, the structures we have studied are organometallic chemical vapor deposition- (OMCVD-) grown GaAs/$Al_{0.3}Ga_{0.7}As$ heterostructures consisting of (from the top of the wafer down, see Fig. 1), an electron injector comprised of an n^+ ($n=2\times10^{18}$ cm^{-3}) GaAs top contact (200 nm), a low-doping ($n=4\times10^{17}$ cm^{-3}) transit region of thickness 250 nm, and an 8-nm AlGaAs tunnel barrier. We follow this with a superlattice transit region consisting of a seven-period superlattice with 12-nm quantum wells and 2.5-nm AlGaAs barriers (the superlattice is terminated at both ends with a GaAs well). The doping throughout the superlattice is n type, $n=2\times10^{18}$ cm^{-3}. Finally, we have an electron spectrometer consisting of a triangular-graded barrier in which we linearly grade the Al concentration to 0.3 over 20 nm and then back down to zero over a further 150 nm. The structure is terminated by a 1000-nm n^+ ($n=2\times10^{18}$ cm^{-3}) region adjacent to a semi-insulating GaAs substrate.[12,13] The wafer was processed using standard wet-etching techniques into mesas of diameter 100 μm, and separate Ohmic contacts were made to the electron injector, superlattice transit region, and electron

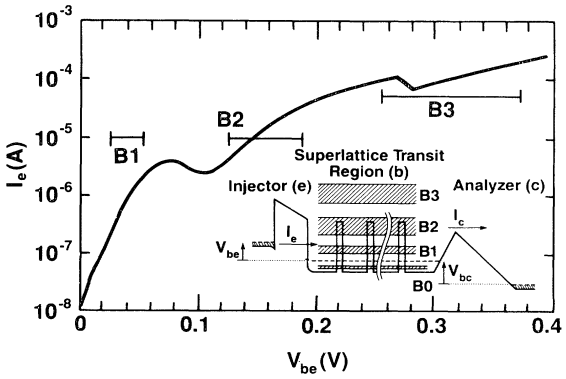

FIG. 1. The injector tunneling characteristic. The calculated effective-mass-approximation minibands are indicated by the solid lines (displaced by the Fermi energy). Inset: Schematic of the structure when typically biased, with the various relevant bias voltages and currents indicated. The minibands are shown hatched; the Fermi energy is shown as a dashed line.

collector using alloyed Au:Sn. Hereafter, we will refer to these contacts as the emitter, base and collector, respectively. The emitter-base bias controls the energy at which electrons are injected into the superlattice, whereas the base-collector bias allows *independent* control of the electron spectrometer. The first four superlattice minibands calculated using Bastard's[14] model are $B0$, 19–26 meV; $B1$, 79–107 meV; $B2$, 176–242 meV; and $B3$, 313–432 meV.

We turn now to the low-temperature (4.2 K) electrical characteristics of the structure. In Fig. 1 we show the injector (emitter-base) characteristic. The presence of two regions of negative differential resistance (NDR) is apparent. Note that in view of the high doping, the bias voltage (in V) corresponds well to the injection energy in the superlattice (in eV). However the large Fermi energy in the superlattice (≈ 80 meV) makes the lowest miniband ($B0$) filled, and therefore, unobservable. We have illustrated the position of the minibands calculated using the Bastard model, displaced by the appropriate Fermi energy, by the horizontal bars in Fig. 1. Although there is a reasonable correspondence between the observed features and the calculated bands, the features are broader than those we have seen in more lightly doped superlattices, probably because of lifetime broadening due to the enhanced plasmon scattering in the highly doped material. The interpretation we will adopt (to be supported by the following measurements) is that between 0.1 and 0.26 V, we are injecting into $B2$; between 0.26 and 0.28 V, we are injecting into the band gap; and above 0.28 V, we are injecting into the third band ($B3$).

Next we will describe the analyzer (base-collector) characteristic under constant-current emitter injection (the emitter-base characteristic is almost independent of V_{bc} implying constant-voltage injection as well). From this we will be able to extract the hot-electron momentum distribution after traversing the superlattice. In Fig. 2(a) we show the collector current as a function of base-collector bias for a sequence of injection energies. As we steadily increase the emitter voltage from 75 to 100 μA, we see an abrupt change in the analyzer characteristic around $V_{bc}=0.1$ V. Reference to Fig. 1 indicates that this corresponds to injection into $B3$. The inference we draw is that when we are biased to inject into $B3$, a quasimonoenergetic electron beam passes through the miniband, and can be detected spectroscopically at $V_{bc}=0.1$ V with the analyzer. We will be more quantitative later.

Of more physical interest is the electron distribution function $n(\epsilon)$ of the electrons after they have traversed the superlattice. By noting that the analyzer only collects electrons with energy exceeding the effective barrier height (at a given bias), it follows that

$$n(\epsilon) \propto \frac{\partial[I_c(I_e) - I_c(I_e=0)]}{\partial V_{bc}}$$

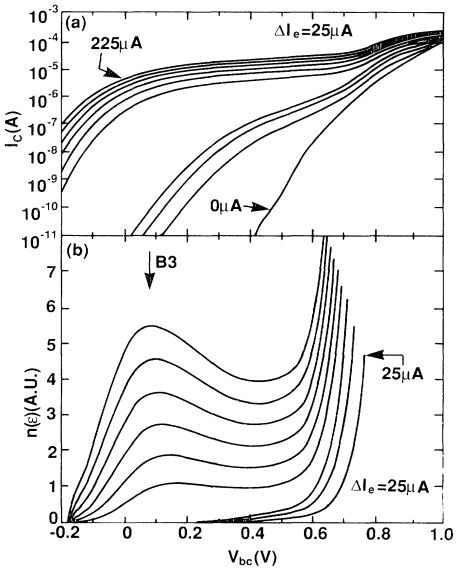

FIG. 2. (a) The analyzer characteristics at a sequence of injector currents (0 μA, 25 μA, 50 μA, etc.) the corresponding injector voltages are V_{be}(mV) = 0, 172, 208, 235, 263, 329, 342, 357, 368, and 376. (b) The electron energy distribution function $n(\epsilon)$ at the same injection energies (omitting 0 mV).

(Ref. 10). We show this derived quantity in Fig. 2(b). [Strictly we are measuring the perpendicular component of momentum, but since most electrons suffer several scattering events we can regard $n(\epsilon)$ as being proportional to the energy distribution.] We see a clear peak in the momentum distribution around $V_{bc}=0.1$ V. *Within the limits of resolution, the peak does not move as the emitter bias (or injection energy) is increased*, giving us confidence that the feature is related to the band structure. This is in contrast to measurements on devices *without* a superlattice in the base, where injection energy and analyzer feature positions are correlated.[15] The appearance of the hot-electron peak is extremely rapid: a >100 times increase in the number of transmitted electrons for a doubling of the injection current. A similar feature is seen when we bias to inject into and sweep through $B2$. In samples in which we intentionally preclude the possibility of band transport by chirping the superlattice period, although we still see structure in the injector, we do *not* see significant hot-electron miniband transport.

An important quantity is the fraction of electrons which transport through the band structure as a function of injection energy: the transfer function, α. We arrive at this parameter by taking the ratio of the analyzer current (at fixed analyzer energy) with the injection current (as a function of injection energy), i.e., $\alpha(\epsilon) = I_c/I_e$, where $\epsilon = eV_{be}$. We have plotted this quantity in Fig. 3 with the analyzer set both to the center of $B2$ ($V_{bc}=0.4$ V, dashed line) and to the center of $B3$

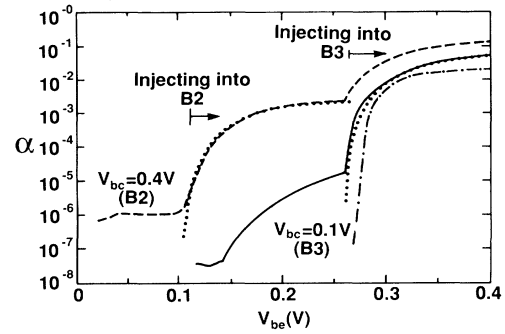

FIG. 3. Fraction of electrons transmitted (the transfer function) with the analyzer set to the center of $B2$ (dashed line) and $B3$ (solid line). The dotted lines are the results of the calculation described using fitted miniband widths, and the dot-dashed line, using the calculated bandwidth.

($V_{bc}=0.1$ V, solid line). Turning first to the characteristic associated with $B2$, we see that for low injection energy (i.e., $V_{be}<0.1$ V), the transfer function is small ($\alpha\approx 10^{-6}$) and independent of bias. However, when biased to inject into $B2$ (i.e., at $V_{be}=0.1$ V), the transfer function rises abruptly, appearing to saturate at $\alpha\approx 3\times 10^{-3}$. A similar feature is seen with the analyzer set to $B3$ (Fig. 3), but now the abrupt change occurs when we bias to inject into $B3$, as we would expect, and the characteristic saturates at $\alpha\approx 0.06$. (With the analyzer set to collect all of the electrons in the ballistic peak, rather than set at its maximum point, we can collect more than 20% of the electrons in the nonequilibrium distribution.) The weaker feature at $V_{be}=0.26$ V with the analyzer set to $B2$, and the nonzero background below 0.26 V in the $B3$ curve are largely a consequence of the finite-energy resolution in the analyzer, which, for example, precludes us from studying the band $B2$ when biased to inject into $B3$.

We will now attempt to explain these observations within the tight-binding approximation of semiconductor superlattices. The excellent energy resolution of the injector (≈ 30 meV) means the transfer function (Fig. 3) can be used as an accurate probe of the miniband dispersion relation. In the following, we will assume a one-dimensional tight-binding miniband dispersion relation $\epsilon(k)=\epsilon_{0i}[1+\cos(ka)]$, where ϵ_{0i} are the miniband half-widths, and a is the period. The use of the infinite-system dispersion relation is clearly only an approximation; however our experimental energy resolution is inadequate for observing the discrete states that comprise the band. The corresponding group velocity is

$$v_g=\frac{\epsilon_{0i}a}{\hbar}\left[\frac{2\epsilon}{\epsilon_{0i}}-\left(\frac{\epsilon}{\epsilon_{0i}}\right)^2\right]^{1/2}.$$

We will now develop a model for electrons propagating in this band structure while scattering and losing energy. We remark that the interband scattering rate is rather low (if the band separation exceeds the optic-phonon energy ϵ_{LO}), because only large-wave-vector scattering events are allowed. Calculations indicate that the interband scattering mean free path is of order 1 μm (away from the band edges), an order of magnitude longer than our superlattice.[12] Therefore, we can consider our electron distribution as confined to a single band. (The eventual fate of electrons close to the band edges will be addressed shortly.) Within a band, we will assume that the predominant energy-loss process is optic-phonon emission described by a single scattering rate τ_{ie}^{-1} for each band.

An electron injected low into the miniband structure will propagate at the appropriate group velocity until scattered or collected by the analyzer; clearly an increased group velocity results in a greater probability of collection and correspondingly higher α. The group velocity increases steeply at the band edges which explains the sudden increase in the transfer function as we bias to inject into a miniband. The group velocity, and hence transfer function, should continue to increase until the band center, whereupon the group velocity starts to fall. However, the transfer function will not fall since an electron injected high in the band, although it will have a shorter mean free path before scattering, is likely to scatter into a state close to the center of the band, where the partial mean free path is again large. Therefore, the transfer function appears to saturate because the electron travels only a short distance in these high-energy states, which is as we have observed. Finally, we expect that electrons close to the band edge will have a very low group velocity, and will not contribute significantly to the current (they may even be in localized states at the band edges), and these electrons will eventually be lost through interband scattering events. We will now give a quantitative description of these phenomena.

Rather than attempting a Monte Carlo or other stochastic description of the transport and energy-loss process, we will use an analytic approach in which we assume that electrons injected at energy ϵ_i can be described as having an average path length $\bar{\lambda}(\epsilon_i)$ before being lost from the band. While within the band, an electron will typically suffer several optic-phonon emissions of energy ϵ_{LO} (strictly coupled phonon-plasmon modes with slightly higher energy). The transfer function may then be written $\alpha(\epsilon_i)=Ce^{-L/\bar{\lambda}(\epsilon_i)}$, where L is the superlattice length and C represents the analyzer efficiency (this is determined predominantly by where we set the analyzer energy, but also is intended to include effects such as scattering events which reverse the electron direction, which we do not describe explicitly, and other events which can remove an electron from the band such as Auger processes). We may express $\bar{\lambda}$ as the sum of the mean free path before scattering and the mean free path after one optic-phonon emission of energy ϵ_{LO}, two

phonon emissions, etc., that is,

$$\bar{\lambda}(\epsilon_i) = \sum_{n=0}^{\text{band edge}} \lambda(\epsilon_i - n\epsilon_{\text{LO}}) \approx \frac{1}{\epsilon_{\text{LO}}} \int_0^{\epsilon_i} \lambda(\epsilon) d\epsilon ,$$

where we approximate a discrete by a continuous energy-loss process (although our bandwidths are only several ϵ_{LO} wide).

Using $\lambda(\epsilon) = v_g(\epsilon)\tau_{\text{ie}}$ and the group velocity described earlier we arrive at the following:

$$\bar{\lambda} = \frac{\tau_{\text{ie}}\epsilon_{0i}^2 a}{2\hbar\epsilon_{\text{LO}}} \left\{ \frac{\pi}{2} + \left(\frac{\epsilon}{\epsilon_0} - 1 \right) \left[2\frac{\epsilon}{\epsilon_0} - \left(\frac{\epsilon}{\epsilon_0} \right)^2 \right]^{1/2} + \arcsin\left(\frac{\epsilon}{\epsilon_0} - 1 \right) \right\}.$$

We have plotted this function using the calculated bandwidth for $B3$ with the dot-dashed line in Fig. 3 (the fitted scattering time is 45 fs). We see that the form of the predicted transfer function is approximately correct in that it predicts the steep rise of α at the band edges, and the form of the saturation near midband. However, if we use the band positions and widths which are more consistent with the injector characteristic, we arrive at the dotted lines in Fig. 3 (the bandwidths chosen are 200 and 300 meV and the fitted scattering times are 24 fs for $B2$ and 21 fs for $B3$, which are close to what we would expect for doped bulk GaAs at these injection energies.[16]). The mean free path before energy loss at the band center given these scattering rates is ≈ 3 periods. The corresponding collection efficiencies, C, are 0.11 and 0.4 for $B2$ and $B3$, respectively. We see very good agreement of the detailed form of the transfer function for realistic values of the fitting parameters (on the logarithmic plot only the scattering rate determines the shape of the curve, and C merely determines the vertical position) suggesting that electrons *are* transporting coherently between scattering events in high-order minibands. A more detailed calculation would necessarily include the anisotropic three-dimensional band structure rather than approximating to a one-dimensional problem.

To conclude, we have described a new type of structure for studying hot-electron effects in semiconductor superlattices. It allows the unique flexibility of independent variable-energy injection into the band structure, *and* spectroscopy on the electrons after they have traversed the superlattice, permitting study of the dynamics of electrons in high-order minibands for the first time. Our results imply that miniband conduction is possible in high-lying minibands: a result vital for device applications of semiconductor superlattices. In addition, our modeling indicates that the electrons are traveling coherently for several superlattice periods between scattering events, and *obey the infinite-system dispersion relation.* Finally, the present type of structure offers the possibility of studying transport in almost any finite artificial one-dimensional potential, and we are currently applying it to other problems including localization and the fabrication of high-gain superlattice-base hot-electron transistors.

We would like to thank S. J. Allen for insightful discussions and critically reading the manuscript, and R. Esagui for technical assistance.

[1]L. Esaki and R. Tsu, IBM J. Res. Dev. **4**, 61 (1970).

[2]F. Capasso, K. Mohammed, and A. Y. Cho, IEEE J. Quantum Electron. **22**, 1853 (1986).

[3]R. Dingle, A. C. Gossard, and W. Wiegmann, Phys. Rev. Lett. **34**, 1327 (1975).

[4]K. K. Choi, B. F. Levine, R. J. Malik, J. Walker, and C. G. Bethea, Phys. Rev. B **35**, 4172 (1987).

[5]T. Duffield, R. Bhat, M. Koza, F. DeRosa, D. M. Hwang, P. Grabbe, and S. J. Allen, Jr., Phys. Rev. Lett. **56**, 2724 (1986).

[6]B. Deveaud, J. Shah, T. C. Damen, B. Lambert, and A. Regreny, Phys. Rev. Lett. **58**, 2582 (1988).

[7]J. F. Palmier, C. Minot, J. L. Leivin, F. Alexandre, J. C. Harmand, J. Danglan, C. Dubon-Chevallier, and D. Ankri, Appl. Phys. Lett. **49**, 1260 (1986).

[8]R. A. Davies, M. J. Kelly, and T. M. Kerr, Phys. Rev. Lett. **55**, 1114 (1985).

[9]P. England, J. R. Hayes, J. P. Harbison, D. M. Hwang, and L. T. Florez, Appl. Phys. Lett. **53**, 391 (1988).

[10]J. R. Hayes, A. F. J. Levi, and W. Wiegmann, Phys. Rev. Lett. **54**, 1570 (1985).

[11]M. Heiblum, M. I. Nathan, D. C. Thomas, and C. M. Knoedler, Phys. Rev. Lett. **55**, 2200 (1985).

[12]D. C. Herbert, Semicond. Sci. Technol. **3**, 101 (1988).

[13]Craig S. Lent, Superlattices. Microstruct. **3**, 387 (1987).

[14]G. Bastard, Phys. Rev. B **24**, 5693 (1981).

[15]J. R. Hayes and E. Colas (unpublished).

[16]J. R. Hayes and A. F. J. Levi, IEEE J. Quantum Electron. **22**, 1744 (1986).